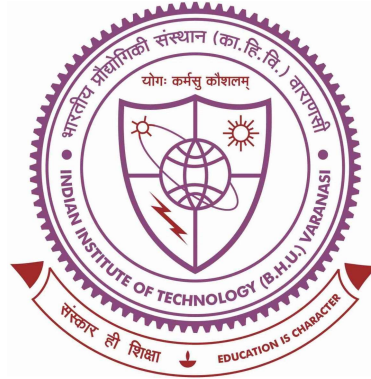


Study of Cool Jets and Evolution of Kelvin-Helmholtz Instability in the Solar Atmosphere



**Thesis submitted in partial fulfillment for the
Award of Degree**

Doctor of Philosophy

by

Balveer Singh

DEPARTMENT OF PHYSICS
INDIAN INSTITUTE OF TECHNOLOGY
(BANARAS HINDU UNIVERSITY)
VARANASI - 221005
INDIA

Enrollment No.: 17171020

2022

CERTIFICATE

It is certified that the work contained in the thesis titled **Study of Cool Jets and Evolution of Kelvin-Helmholtz Instability in the Solar Atmosphere** by **Mr. Balveer Singh** (Roll No. **17171020**), in partial fulfillment of the requirement for the award of the degree of Doctor of Philosophy at the **Indian Institute of Technology (B.H.U.), Varanasi** is a record of his own work carried out under my supervision and guidance and this work has not been submitted elsewhere for a degree.

It is further certified that the student has fulfilled all the requirements of Comprehensive Examination, Candidacy, and SOTA for the award of Ph. D. Degree in Physics.

Abhishek K. S.
20/11/2022

Supervisor **Associate Professor**
(Abhishek K. Srivastava) **Department of Physics**
Indian Institute of Technology
(Banaras Hindu University)
Varanasi-221005
Associate Professor
Department of Physics
Indian Institute of Technology
(Banaras Hindu University)
Varanasi-221005

Declaration

I, **Balveer Singh** (Roll No. **17171020**), certify that the work embodied in this thesis is my own bonafide work and carried out by me under the supervision of **Dr. Abhishek K. Srivastava** from July 2017 to August 2022 at the *Department of Physics*, Indian Institute of Technology (BHU), Varanasi. The matter embodied in this thesis has not been submitted for the award of any other degree/diploma. I declare that I have faithfully acknowledged and given credits to the research workers whenever and wherever their works have been cited in my work in this thesis. I further declare that I have not wilfully copied any other's work, paragraphs, text, data, results, *etc.*, reported in journals, books, magazines, reports dissertations, thesis, *etc.*, or available at websites and have not included them in this thesis and have not cited as my own work.

Date 20/12/2022

Signature

Place IIT (BHU), Varanasi Balveer Singh

CERTIFICATE BY THE SUPERVISOR

It is certified that the above statement made by the student is correct to the best of my knowledge.

Supervisor

Dr. Abhishek K. Srivastava
Associate Professor
Department of Physics
Indian Institute of Technology
(Banaras Hindu University)
Varanasi-221005

Signature of the Head of the Department
विभागाध्यक्ष / Head
भौतिक विभाग / Deptt. of Physics
भारतीय प्रौद्योगिकी संस्थान /
Indian Institute of Technology
(का०हि०वि०) / (BHU)
वाराणसी / Varanasi-221005

COPYRIGHT TRNSFER CERTIFICATE

Title of the Thesis: "Study of Cool Jets and Evolution of Kelvin-Helmholtz Instability in the Solar Atmosphere"

Name of the Student: Balveer Singh

Copyright Transfer

The undersigned hereby assigns to the Institute of Technology (Banaras Hindu University) Varanasi all rights under copyright that may exist in and for the above thesis submitted for the award of the "*Doctor of Philosophy*".

Date 20/12/2022

Signature



Place IIT(BHU), Varanasi Balveer Singh

Note: However, the author may reproduce or authorize others to reproduce material extracted verbatim from the thesis or derivative of the thesis for author's personal use provided that the source and the Institute's copyright notice are indicated.

In the Honour
of
My Loving Family

Acknowledgements

First and foremost, I would like to express my gratitude and deepest appreciation to Dr. A.K. Srivastava whose friendly guidance, care, help and supervision enabled me to complete my Ph.D. thesis. His constant support, encouragement, discussions and inestimable suggestions kept me moving on the path to becoming a good researcher.

It is my pleasure to thank the Human Resource Development Group (HRDG), Council of Scientific & Industrial research (CSIR) India, to provide me the financial assistance for the current research. I would like to thank to the members of Research Progress Evolution Committee (RPEC), especially Dr. Prasun Dutta and Dr. Vineet Kumar Singh for their constructive comments on several presentations during my Ph.D. program. I would like to express my gratitude to Prof. Bhola N. Dwivedi for his encouragements. I would like to express my gratitude and thankfulness to Prof. K. Murawski, UMCS, Lublin, Poland for his discussions and support, as well as providing a module related to the realistic solar atmosphere. I would like to thank all the faculty members of the Department for their logistic support. I am also thankful to all the non-teaching staff of the Department for their assistance when needed.

I also thank my co-authors from whom I have learnt considerably. I wish to thank my colleagues (Pradeep Kayshap, Ritika Solanki, Sudheer K. Mishra, Yamini K. Rao, Kartika Sangal, Shweta Didel, Srikar Paavan T, Sripan Mondal, Kushagra Sharma) of the Solar Physics group in the Department for their help, support and several productive discussions.

I would like to thank my friends (Abhay, Abhishek Kr. Singh, Rohit, Alam, Gurudev Nirala, Prashant Pandey, Prashant Dixit, Digvijay, Vaibhav, Vivek, Suraj, Raj, Manish, and

junior or senior colleagues) for their friendly support. I wish to special thank to my other friends (Shubhi, Abhijeet, Deepak, Abha, Divya, Amit) for their moral support.

I would like to express my grateful thanks to my parents, my brother and sister-in-law (Mr. Krishna M. Singh & Mrs. Babita) for their unconditional love, blessings, patience, care, and supports in countless ways. I would like to special thank my sister (Mrs. Sima Singh) for blessings, love and constant support. I also thank to other siblings (Ragini, Pravin, Navin, Kajal, Sikha, Soni and Adhish) for their love and support. I am also blessed to have my cute niece (Amrita) for being such a bundle of joy in my life. I would like to specially thank Mrs. Shobhna Ma'am for her encouragements, blessings and moral support.

Finally, I wish to thank one and all for extending their cooperation directly or indirectly.

Department of Physics, IIT (BHU)

Balveer Singh

Preface

Human nature has always been fascinated about ongoing events in the natural world. As a result of this curiosity, many things have been discovered, and mankind have been able to explain a variety of natural phenomena occurring around themselves and in their nearby space. This leads to the development of basic sciences, which in turn caused the growth of human civilization. The development in the basic science and its understanding is further translated into the relevant technological developments.

We know a lot about the cosmos from past research since it contains a millions of stars, planets, and other similar objects that form galaxies, and there are a millions of galaxies in the universe. Today, the technology have advanced to a point where we can now investigate far-flung parts of the universe (e.g., galaxies, Sun and Sun like stars, planets etc.) revealing a range of exotic physical processes at disparate spatio-temporal sizes and energy levels. In the frame-work of astronomy and astrophysics, technological and scientific advancements have provided more insight into the dynamics and formation of interstellar medium, nebula regions, galactic, active galactic nuclei (AGNs), black holes, supernovae, various types of stars, planets, and other massive energetic objects. These modern technologies have revealed that 99.99 percent of the particles in the universe are in the plasma state, which is always in motion. These accomplishments help us to advance many other area of research while also bringing in a wide range of new technologies to the mankind, such as detector technology and improved sensitive cameras, modern optics, cutting-edge software etc. With the appearance of telescopes a few millennia ago, the first object in the near by space, our parental star "The Sun," was explored in greater details. People's impression of the Sun is that it is a source of light and heat and supports our life on the Earth. Scientifically, It's estimated that the Sun is 4.2 billion years old, and it is a magnetically active young star that is in the middle of its life cycle. Furthermore, the Sun's conditions are so dynamic and

complicated that our intuition frequently fails to forecast their precise causes. As a result, many physical processes at the Sun were not predicted prior to their observation, and we continue to strive to comprehend them. These physical processes take place on spatial and temporal scales that are too enormous to investigate under terrestrial conditions, and they are too complex to numerically simulate. Our parent star has a vast spectrum of physical processes in its electrically conductive plasma with mass density and temperature varying by many orders of magnitude and spatial scales ranging from atomic to hundreds of Mm.

The Sun's complex magnetic structuring, which is formed by appropriate dynamo action, has been discovered to impact the dynamics of its numerous gaseous atmospheric layers (e.g., photosphere, chromosphere, transition layer, and outermost layer, corona). These complex/complicated motion of the particle fluid at the Sun are responsible for the formation of waves, small-scale transients, various eruptions, all electromagnetic radiation, and the emission of high-energetic particles that make up the Sun-Earth connection, heliospheric environment, and interplanetary magnetic fields. These ejected radiations, high energetic charged particles, explosive plasma eruptions, and supersonic flows enter into the Earth's upper atmosphere (e.g., ionosphere, magnetosphere) that are responsible for the powerful solar storms. These high potential solar storms have the ability to damage space satellites that we rely on for navigation and communication system. It can also cause possible threats to the space stations, astronauts, Earth's satellites as well as impair power networks that provide our electricity, air-travel, and communication. Therefore, these events/effects can be predicted by studying space weather candidates like eruptive prominences, coronal mass ejections, and solar flares. Recently, significant observational studies demonstrated that multiwavelength emissions from various parts of the Sun, reveal the dynamics of many small-scale transients/eruptive processes and their physical ramifications. As per modern technology, understanding the physical mechanism of such events

is required in order to apply rigid constraints to numerous transients/eruption models, allowing scientists to better understand and anticipate the mechanism of transients/eruptive processes and their spread in the heliosphere. As a result, these active stars, which have a hot plasma and a denser magnetized atmosphere, produce magnetic waves and explosive eruptions on a wide scale, which affect the weather in space. The relationship between the Sun and the Earth was established when such high-energy dynamical magnetic fields reconnected with planetary magnetic fields (e.g., Aurora etc.) and enter the high-energy particles and radiation in the Earth's atmosphere. However, not only the interplanetary space is influenced, but the Sun's strong magnetic fields affect cosmic bodies on both large as well as small scales. Therefore, Earth's magnetic fields habitable as a magnetic protection from the Sun's highly dynamic magnetic fields and high-energy radiation and particles.

The dynamics and characteristics of different layers differ greatly, making the Sun more fascinating. Its various atmospheric layers are complex in terms of magnetic and plasma structuring. The complex structure and highly dynamic nature of its atmosphere often limits our scientific ideas to predict the exact causes of energy and mass transport, and transient processes that take place in its atmosphere. As far as we know, the photosphere and chromosphere have temperatures ranging from 4300 K to 10000 K. The temperature abruptly increases as moves near the transition region, which is about a few hundreds kilometers thick, and reaches millions degrees Kelvin in the outermost layer i.e., corona. The large temperature difference between the photosphere and the corona violates the standard laws of thermodynamics, posing a challenge for cutting-edge researchers. This is the one of a big mystery for the solar scientists. Therefore, understanding of the physical processes for heating and mass transport may significantly contribute to the development in understanding the dynamics of the solar atmosphere, its connection to the heliosphere. Another key question in heliophysics is how solar wind originates and accelerates from

the solar atmosphere, which is addressed in this order. In the field of solar physics, this is likewise an unsolved problem.

The another fundamental question concerns how the mass cycle and its transformation with supersonic speed in the solar atmosphere is well established. These fundamental questions raise greater concerns for solar scientists for few decades. Despite the fact that there are two types of physical processes that deal with the aforementioned problems, one relating to direct current dissipation in the magnetic plasma known as magnetic reconnection and second is conveying energy in the form of an alternating current source associated with magnetic waves, none of them fully explain the aforementioned fundamental problems. These two mechanisms (magnetic waves and magnetic reconnection) helps to understand about all possible dynamical plasma processes in the Sun's atmosphere. These fundamental plasma processes also deals the energy and mass transport from photosphere to corona coupling various layers at disparate scales. Therefore, the small and large scale transients and eruptive processes and their association with planetary space, occur in the highly dynamic, and million-degree hot solar atmosphere reveled by the physical plasma processes which are based on the magnetic reconnection and magnetic waves. The supply of mass and energy into the upper layer from the solar chromosphere via heat flow, solar winds, cool jets, spicules and other plasma ejecta maintained the energy balance in the solar atmosphere. The magnetic reconnection and various kind of MHD waves are fundamental processes that deals the localized atmospheric heating coupling various layers of the Sun's atmosphere.

Recently, various extensive high-resolution space-borne and ground based observatories (e.g., Solar and Hemispheric Observatory (SOHO), Interface Region Imaging Spectrograph (IRIS), Solar Dynamics Observatory (SDO) etc.) reveled transportation of mass and carry

energy which described the subsequent localized heating. The observations from these instruments also reveal that coronal holes have various flux tube-like structures anchored in the solar photosphere's strongly magnetic regions. Therefore, the plasma flows and jet like plasma ejecta also occur from the footpoint of these flux tube like structures in the solar atmosphere. Solar active regions, which have a high magnetic field and complicated plasma processes, also play an important role in localized heating. In the solar active regions, magnetic loop-like structures emerged at various scales, which is connected with localized heating via various plasma processes such as global energizing, p-mode leakage, Alfvén wave mode conversion etc. The active regions above sunspots, consist of hot plasma flows, diverse MHD waves and oscillations, shocks, and complicated plasma dynamics which may be triggered by the magnetic reconnection. Another aspect of the locally plasma flows, waves and dissipation of magnetic topology occur in the solar atmosphere which are subsequently described the localized heating.

Although, for two decades, several high-resolution instruments (e.g., IRIS, SDO, SST, ROSA, 4m-DKIST, Solar Orbiter and Parker's Solar Probe etc.) have been already addressed a variety of small scale transient and wave processes and have ability to determine the various plasma properties of the Sun's atmosphere currently, yet the cutting-edge scientists and researchers developing more observational facilities (e.g., 4m-DKIST, 1m-SST at La Palma, 4m-EST, 2m-NLST, (upcoming) Solar Orbiter etc.) to anticipate deeply about these plasma processes at very fine scales in the solar atmosphere. In this series, Indian space agency (ISRO) is also developing the solar space mission, Aditya-L1, to contribute in the deep understanding about these small scale plasma processes at high cadence. Aditya-L1, carry the various instruments such as SUIT, etc to established the observations of the various plasma processes of the Sun's lower atmosphere at finer scales. Therefore, Aditya-L1 has substantial scientific goals in the frame-work of studying the

waves/ shocks/ magnetic reconnections/plasma flows, plasma ejection and their associated plasma processes which helps to understanding the localized coronal heating and mass transport. Therefore, the developing/upcoming solar missions will more capable to answer the fundamental problems such as coronal heating, origin of solar wind and its acceleration, and how the mass and energy transport into the upper region of solar atmosphere occur.

In analogy, it may also be very significant in understanding the various plasma processes at laboratory scale. In particular, several models were presented to understand localized plasma flows and ejecta such as solar jet, spicules, and their associated plasma dynamics that responsible for enforcing the energy and mass supply from the lower solar atmosphere to the inner corona is the main body of this thesis. In order to make numerical simulations and observations of solar chromospheric jets, associated waves, oscillations and instabilities give a better insight onto the problems of chromospheric/coronal heating, associated energy and mass transfer coupling the quiet solar atmosphere. The results of the scientific works included in this thesis, will help to explain the various plasma dynamics occurring in the solar atmosphere, and formulated theories for interpretation of the current as well as future solar observations (e.g., SST, ROSA, DKIST, EST, Indian NLST, Aditya-L1) that identify the main energy sources in the Sun's atmosphere. The complex structuring and highly dynamical nature of the Sun's atmosphere allows the triggering of various localized transient plasma processes (e.g., spicule-like jets, network jets, mottles, dynamic fibrils, surges etc). These spectacular plasma jets/flows could be responsible for transporting mass and energy in the overlying solar atmosphere. Such plasma jets may also be associated with various types of waves and oscillations, shocks, and instabilities. Understanding the formation, dynamics, and energetics of these solar jets are the front line scientific problem in the area of solar physics. For a complete comprehension of the mass and energy transport in the Sun's atmosphere, these solar jets must be understood

quantitatively using the models and observations.

Solar jets are high-velocity plasma ejections that are impulsive and collimated along the magnetic field lines in the Sun's atmosphere. Small-scale cool jets ($T < 10^5$ Kelvin) and associated plasma dynamics have been detected in multiwavelength observations using various ground and space-borne observatories. Their physics can be understood in depth by performing the numerical modelling using theory of magnetohydrodynamics (MHD). In this thesis, we have described few extensive MHD models in ideal and non-ideal regime that demonstrate origin and evolution of these cool jets and associated plasma processes. Our findings are consistent with various observations of cool solar jets. These scientific findings are helpful in understanding the intricate relationship between plasma flows and complex structuring of magnetic field leading the evolution of various triggering processes of these jets in the solar atmosphere. This also provides clues of their significant role in energy and mass transport into the lower solar corona.

This thesis aims to provide the physical understanding of jet-like plasma features in the dynamic magnetic solar atmosphere. These cool jets are often triggered from the chromospheric layer and observed on the solar limb and also on the solar disk. These jets have been observed in both in the active and quiet regions of the Sun's atmosphere. These small scale spicule-like plasma motions have been recorded with a notion of their quasi-periodic rise and fall in the Sun's atmosphere at diverse spatio-temporal scales. The different incarnations of plasma are revealed in these jets. More-specifically, we address the formation of such spicule-like cool jets and associated plasma dynamics using 2-D and 2.5-D MHD modelling. The triggering mechanism (driver), dynamical evolution, kinematics, and energetics of such plasma ejecta in the solar atmosphere are the main theme of this thesis. While, all the chapters (Chapters 3-6) are basically related with the MHD model of

the jet evolution and its dynamical behaviour, the Chapter 7 demonstrates specifically the observations of a cool coronal jet possessing the Kelvin-Helmholtz Instability. The present thesis is organized in form of the following chapters:

Chapter 1: Introduction of the Sun and Its Atmosphere

In this chapter, we discuss a brief overview of the Sun and its different layers particularly both in its interior and exterior. We outline the Sun's localized magnetic field and the facts that how they relate to various transient plasma processes. We give a succinct overview of the solar jets and associated plasma processes on the basis of various ground and space-borne observations as well as theoretical and numerical models. At the end we append the structure of the present thesis and its various chapters.

Chapter 2: Overview of the Observational Data, Analysis Techniques and Numerical Methodology

In this chapter, we briefly elucidate on various space-borne observatories and onboard instruments whose data were used to study the solar cool jets at diverse spatio-temporal scale as outlined in Chapter 5 and 7. We also discuss data calibration tools and analysis techniques. At the end, we describe the numerical simulation method and techniques used in the modeling of these cool jets.

Chapter 3: Spicule-like Cool Jets Driven by Alfvén Pulses in the Solar Atmosphere

In this chapter, we have discussed the detailed mechanism of the formation of spicule-like cool jets driven by Alfvén pulses using 2.5D ideal MHD simulation. These spicule-like cool jets are triggered in the solar atmosphere by initial implementation of multiple transverse velocity pulses in the z -direction (i.e. V_z), which mimic the Alfvén pulses. We found that if the transverse velocity pulses have a large enough amplitude (50–90 km s⁻¹), they

produce field-aligned magnetoacoustic perturbations in the solar chromosphere through Ponderomotive force, which is later responsible for the formation of spicule-like cool jets. The Alfvén pulses were implemented at chromospheric heights between 1.5 and 2.0 Mm. The evolution, kinematics, and energetics of these spicule-like jets are investigated. We found that transported massflux and kinetic energy density are significant to fulfill the localized coronal losses. These mass motions cause *in-situ* quasi-periodic oscillations of the period of 4.0 min in the transition region.

Chapter 4: Kinematics and Evolutionary Properties of Impulsive Jets Driven by Pressure Pulse in the Solar Atmosphere

In this chapter, we have discussed the kinematics and evolutionary properties of impulsive cool jets in the Sun's atmosphere using 2-D numerical simulation at two different magnetic field strengths ($B=56$ gauss and $B=112$ gauss) of the quiet-Sun. These cool jets originate due to pressure pulses implemented at the chromospheric height (1.8 Mm), which mimics the after-effects of the localized heating in the solar chromosphere. We studied the parametric behaviour of these cool jets in the gravitationally stratified model atmosphere with realistic temperature model. This model suggests that pressure pulse is sufficient to produce the required perturbations in the middle chromosphere to launch the cool jets in the solar atmosphere.

Chapter 5: Impulsive Origin of Spicule-like Jets in the Solar Atmosphere

In this chapter, we studied the impulsive origin of cool jets which is previously observed by Chen et al. (2019) using high-resolution spectroscopic observation of the coronal hole in Si IV 1393.755 Å line recorded from Interface Region Imaging Spectrograph (IRIS) on 8th October 2013. The non-Gaussian line profiles show unusual line broadening, which correspond to the plasma velocity enhancement. We revisit the observations of Chen

et al. (2019) with a new method of spectral fitting, and analyze a specific event associated with a cool jet. The non-Gaussian profiles in the Si IV 1393.755 Å line, for a lifetime of 3.0 min and Doppler shifts reaching 68 km s^{-1} , is associated with a spicule-like jet of length 8.0 Mm. We model this jet by implementing the observed velocity enhancement in a magnetized and gravitationally-stratified solar atmosphere. The velocity perturbation of 68 km s^{-1} , resembling the observed velocity enhancement, launches a thin spicule-like jet whose properties closely match with the observed jet. We also show that non-adiabatic conditions (e.g., thermal-conduction and radiative-cooling) affect the jet propagation, mass flux, and kinetic energy density. We found that these jets transport mass and energy into the overlying atmosphere. It also demonstrates that the cooling atmosphere affects the kinematics and energetics of the jets.

Chapter 6: Decaying Kink Oscillations in the Fine-structured Cool Solar Jets

In this chapter, we perform a 2-D magnetohydrodynamic (MHD) simulations that provide a detailed picture of the evolution of cool jets caused by initial vertical velocity perturbations in the solar chromosphere. We implement random multiple velocity (V_y) pulses of amplitude $20\text{-}50 \text{ km s}^{-1}$ between 1.5 and 2.0 Mm in the solar atmosphere below the transition region (TR), which subject to the different switch-off period for the phase of the perturbations between 50-300 s. These applied vertical velocity pulses create series of magnetoacoustic shocks steepening above TR, and interacting with each other in the inner corona leading a complex localized velocity fields. The propagation of such perturbations create low-pressure regions behind and generate a variety of cool jets and plasma motions. We aim to study the oscillations of two cool jets J_1 and J_2 that move upto the height respectively 6.2 Mm and 5.4 Mm above TR. These jets are fine-structured radially in density and Alfvén speed. The highly dense J_1 , which triggered along the significantly curved magnetic field lines, support the propagating transverse kink waves of period ≈ 195 at a

speed of $\approx 125 \text{ km s}^{-1}$. In the case of J_2 , the evolved collective kink oscillations no longer sustain beyond its one cycle, and dissipated quickly. At the later stage, instead of collective oscillations of jet's spine, its outer surface possesses transverse oscillations locally without significantly perturbing the inner core of the jet. The different fine structures of the jet's spine oscillate locally in a transverse manner especially near the surface. We describe that the radial structuring of density and characteristic Alfvén speed within J_1 and J_2 , as well as the curvature of the magnetic field cause onset of the resonant conversion and leakage of the wave-energy outward to dissipate these transverse oscillations.

Chapter 7: Kelvin–Helmholtz Instability in the Cool Plasma Jet in the Solar Atmosphere

In this chapter, we have studied the development of the Kelvin–Helmholtz (K–H) instability in the jet-like cool plasma ejection using EUV observations taken from SDO/AIA instrument on 2015 March 10. This plasma ejection resembles a jet-like flow and is located close to an active region (AR 12279) with a fan-spine structure rooted in a nearby sunspot. We found that this fan-spine configuration contains both cool and hot plasma simultaneously. However, we emphasize here the dynamics of the cool plasma component of the jet. The magnetic configuration consists of two layers of cool plasma, which flow in parallel and interact with one another inside the extended spine. The impulsive plasma flows upward with a speed of $114\text{--}144 \text{ km s}^{-1}$ from below and interact with the slower plasma flow (5 km s^{-1}) that is the reflected stream along the spine's field lines from the top. This process causes a shear motion around the outer spines, which then causes the K-H instability to evolve and seen in comparatively cooler plasma. We also show the cause of the velocity difference between two layers. The velocity of K-H unstable vortices, are greater than the Alfvén speed in the second denser layer, satisfying the criterion of K-H instability growth. Our finding suggests that the fan-spine topology may rapidly heat up in

the presence of complex structuring of magnetic field and plasma flows.

Chapter 8: Conclusions and Future Plan

In this chapter, we focus on the summary of scientific works presented throughout this Ph.D. thesis. In the conclusion, we summarize our results and provide some valuable remarks for future observational capabilities from the current/upcoming national and international space and ground based observatories and their various instruments (e.g., IRIS, SDO, Solar Orbiter, upcoming Aditya-L1, Solar-C, SST, ROSA, DKIST, EST, upcoming Indian NLST etc), and model simulations supporting the novel observational findings. Our findings will be utilized to explain the physics of cool jets in the Sun's atmosphere, as well as to provide a theoretical foundation for interpreting present and future solar observations. It will also help in understanding the mechanisms of the primary energy sources and mass transport as well as the fundamental physical processes (e.g., waves, instabilities, confined flows, etc) in the localized solar atmosphere.

Table of contents

List of figures	xxix
List of tables	xliii
Nomenclature	xliii
1 Introduction of the Sun and Its Atmosphere	1
1.1 Overview of the Sun	2
1.1.1 Interior of the Sun	3
1.1.2 The Solar Magnetic Field	7
1.1.3 Exterior of the Sun	10
1.2 Solar Jets: A Brief Overview	18
1.3 An Observational View of Chromospheric Jets	21
1.3.1 Spicule-like jets	22
1.3.2 Macrospicule	25
1.3.3 Dynamic fibrils	26
1.3.4 Mottles	26
1.3.5 Network jets	27
1.3.6 Other cool jet-like structures	28
1.4 Solar Chromospheric Jets: Theoretical and Numerical Understanding . .	28
1.4.1 Magnetic reconnection models	28

1.4.2	Alfvén wave models	30
1.4.3	Acoustic wave models	32
1.4.4	Pressure pulse model	34
1.4.5	Effect of the non-ideal processes	35
1.5	Evolution of Dynamical Processes in Jets	36
1.5.1	Oscillations in the jets	36
1.5.2	Instability in the jets	37
1.6	Outline of the Thesis	38
2	Overview of the Observational Data, Analysis Techniques and Numerical Methodology	41
2.1	Observational Perspectives of the Solar Atmosphere	42
2.2	Space-based Observatories	44
2.2.1	Interface Region Imaging Spectrograph (IRIS)	44
2.2.2	Solar Dynamics Observatory (SDO)	47
2.3	Data Analysis Techniques	51
2.3.1	Image calibration and data processing	51
2.3.2	Spectral analysis	52
2.3.3	Differential emission measure (DEM) analysis	53
2.4	Numerical Methods	55
2.4.1	Magnetohydrodynamic (MHD) system	55
2.4.2	Structure of PLUTO code	58
2.4.3	Solenoidal constraint	60
2.4.4	Notations and grids	61
2.4.5	Reconstruction	62
2.4.6	Riemann solver	63
2.4.7	Temporal evolution	65

2.4.8	Source terms and non-hyperbolicity	67
2.4.9	Units and dimensions	69
2.5	Wavelet Analysis Technique	70
3	Spicule-like Cool Jets Driven by Alfvén Pulses in the Solar Atmosphere	73
3.1	Introduction	74
3.2	Basic Model of the Solar Atmosphere	78
3.3	Numerical Methods	83
3.4	Perturbations	85
3.5	Generation of Spicule-like Cool Jets Driven by Alfvén Pulses and Their Properties	88
3.6	Discussion and Conclusions	98
4	Kinematics and Evolutionary Properties of Impulsive Jets Driven by Pressure Pulse in the Solar Atmosphere	103
4.1	Introduction	104
4.2	Basic MHD Model of the Pressure Pulse Driven Jets	107
4.3	Perturbations	113
4.4	Numerical Methods	116
4.5	Generation of Cool Jets Driven by the Pressure Pulses and Their Properties	116
4.6	Discussion and Conclusions	123
5	Impulsive Origin of Spicule-like Jets in the Solar Atmosphere	125
5.1	Introduction	127
5.2	Observations	132
5.3	Numerical Model of the Spicule-like Jet in Energy Imbalance Condition in the Solar Atmosphere	136
5.4	Perturbations	140

5.5	Numerical Methods	143
5.6	Evolution of Spicule-like Cool Jets and Their Properties	146
5.7	Discussion and Conclusions	157
6	Decaying Kink Oscillations in the Fine-structured Cool Solar Jets	165
6.1	Introduction	166
6.2	Numerical Model of the Generation of Oscillating Spicule-like Cool Jets .	170
6.3	Numerical Methods	173
6.4	Perturbations	175
6.5	Evolution of the Transverse Kink Waves in the Cool Jets	180
6.6	Discussion and Conclusions	183
7	Kelvin–Helmholtz Instability in the Cool Plasma Jet in the Solar Atmosphere	185
7.1	Introduction	186
7.2	Observational Data and Analyses	190
7.3	Observations of K-H Instability and Its Theoretical Interpretation	193
7.4	Discussion and Conclusions	205
8	Conclusions and Future plan	209
8.1	Summary and Conclusions	209
8.2	Future Plans	212
	Bibliography	215
	Appendix List of Publications	247

List of figures

- 1.1 An illustration about the various parts of the Sun. The solar interior is categorized as core, radiative zone and convection zone. The central region of the Sun is known as core where nuclear fusion reaction takes place. The radiative zone is a layer from where the generated energy from the core is propagating outward in form of the radiation. The convection zone is a part of the solar interior from where the energy propagates up to the Sun's surface due to convection. The Sun's surface (i.e. photosphere), chromosphere, corona are shown. The sunspots, coronal loops, solar flares and eruptive prominence belong to different atmospheric layers of the solar exterior (Credit: NASA/anatomy of the Sun). 4
- 1.2 The differential rotation of the extensively conductive and rotating plasma gas revolving with the magnetic field in the Sun's interior. The magnetic polarity reverses between the two hemispheres. (Credit: Addison Wesley). 7
- 1.3 A schematic of the quiet-Sun's atmosphere. This shows the inside and outside strongest magnetic field intensity in magnetic networks exhibiting multiple physical processes coupling various parts of solar atmosphere. The magnetic field lines are shown by the solid and dotted black lines. The height range that ALMA mapped is shown in the left (Credit: S. Wedemeyer-Böhm) 9

-
- 1.4 The temperature and density variations with height in the solar atmosphere (Credit: Eugene Avrett; Smithsonian Astrophysical Observatory). 10
- 1.5 The left panel shows the full-disk visual surface of the photosphere. The right panel shows the magnified regions of the particular features of strongly magnetized active region (AR) sunspot surrounding the quiet-Sun (QS) granules (Credit: Hinode, S. Tsuneta, NAOJ, JAXA, and NASA). . . 11
- 1.6 The Maunder butterfly diagram and variation of the sunspots on the solar disk. Top panel represents the area of sunspot with latitude and time. Bottom panel shows the data appears monthly averages of daily sunspot numbers which is a function of time (Credit: Hathaway 2022). 11
- 1.7 Left: The chromospheric layer with plage and filament magnetic structures. Right: The photospheric layer with sunspots and faculae (Credit: NASA/GSFC, Source data courtesy of HAO & NSO PSPT project team). 14
- 1.8 Left: An eruptive large prominence is observed in He II 304 Å with a comparative picture of the Earth. (Courtesy: Solar and Heliospheric Observatory (SOHO)/ EUV Images Telescope (EIT); Big Bear Solar Observatory). Right: The magnetic loops of the solar active region are observed above the solar disk as detected by the Transition Region and Coronal Explorer (TRACE) on September 28, 2000. (Credit: M.Aschwandhan, LMSAL, TRACE, and NASA). 15
- 1.9 Multiwavelength observations of the solar flare on May 5, 2015. The flare is shown at different wavelengths from left to right at visible waveband, 171, 304, 193, and 131 Å (Credit: NASA/SDO/Wiessinger). 15
- 1.10 Left: coronal helmet streamer, and pseudostreamer. Right: CME seen with the LASCO instrument in the C2 coronagraph during total solar eclipse (Credit: NASA/COSMOS). 17

-
- 1.11 A typical coronal jet in the quiet-Sun atmosphere at the solar limb on July 7, 2014 at 14:16 UT observed with multiwavelength SDO/AIA channels (Credit: JHelioviewer; SDO/AIA, LMSAL). 19
- 1.12 The thread-like features visible in this field-of-view as seen from the Japanese satellite Hinode are solar spicules. These ejecta are the plumes of gas transporting energy and mass into the localized solar atmosphere. (Credit: NASA /JAXA). 23
- 1.13 The hot component of spicule-like chromospheric jets are detected using AIA 304 Å (upper-left panel) and 193 Å filters (upper-right panel). The cyan square represents the SST CRISP field of view. The bottom panels display same structures in Ca II H (left) and $H\alpha$ (right) as observed by Swedish Solar Telescope (SST). The red arrows show the bidirectional flow of plasma as a spicule-like jets. This observations is taken on June 17, 2014 at 10:30 UT. Radially filtered $H\alpha$ and Ca II H images have been used to make spicules more visible. (Credit: Pereira et al. 2016). 24
- 1.14 Observation (bottom), and simulation (top) of the spicule-like jets. (Credit: University of Oslo/Swedish 1-m Solar Telescope). 29
- 1.15 The snapshots show the temporal evolution of cool jets in two-fluid model (ions+neutrals). The logarithm of density map of ions are shown at $t=70$ s, 210 s, 320 s (from top-left to top-right), whereas snapshots from bottom-left to bottom-right display the logarithm of density map of neutrals at the same time. Ion and neutral velocity vectors are shown by arrows in x-y plane. On the colormap, the warm coronal plasma is represented by blue color, the cool chromospheric plasma by orange-red, and the plasma in the transition region as green (Credit; Kuźma et al. 2017b, ApJ, IOP publishing). 31

1.16	Time-distance map of spicule-like jets as shown in temperature (T) and mass density (ρ). The solid line represents the position of plasma beta equals to 1. The transition region ($T = 40,000$ K) is shown by the dashed line (Credit: Iijima 2016).	33
2.1	Interface Region Imaging Spectrograph (IRIS) with two instruments namely slit-jaw imager, and spectrograph (Credit: LMSAL, NASA/IRIS)	45
2.2	Solar Dynamics Observatory (SDO) spacecraft with it's three instruments i.e., AIA, EVE, and HMI (Credit: NASA/SDO).	48
2.3	SDO/AIA observation of the Sun's atmosphere in EUV/UV and visible wavebands. (Credit: NASA/SDO).	49
2.4	The reconstruct-solve-average (RSA) approach is depicted in a flow chart as originally given in Mignone et al. (2007a). Top-left: Volume averages (\mathbf{U}) is easily converted into primitive variables (\mathbf{V}). Top-right: The left and right states are respectively represented by ($\mathbf{V}_{+,L}$) and ($\mathbf{V}_{-,R}$) using either extrapolation or interpolation of appropriate variables. The solution is therefore advanced and updated in time by solving a Riemann problem between states ($V_{+,L}$) and ($V_{-,R}$). It further computes the numerical flux function (F_+) at various interfaces of the given cell (Mignone et al., 2007a). This scheme is adopted from the master paper of PLUTO by Mignone et al. (2007a).	59
3.1	Left: The open expanding magnetic field lines are shown in the stratified solar atmosphere at equilibrium. The source magnetic pole is kept at -3.0 Mm below the boundary of the solar photosphere at $x=0$ Mm. The magnetic pole strength is taken as $\simeq 560$ G. Right: The temperature profile w.r.t. the vertical height of the solar atmosphere is displayed as per the model given by Avrett and Loeser (2008).	79

3.2 The magnetic field (top-left), plasma beta (top-right), pressure (middle-left), mass density (middle-right), Alfvén speed (bottom-left), and sound speed (bottom-right) w.r.t. height (y) are displayed in the model solar atmosphere. 81

3.3 The normalized density map of the evolution of different spicule-like jets are shown in this figure. These jets are triggered due to 15 different amplitudes of the V_z pulses. The transverse pulses mimic the Alfvén pulses which are applied in the chromosphere between 1.5 and 2.0 Mm. The amplitude of these pulses lie between 50 to 90 km s^{-1} . They generate the field aligned magnetoacoustic shocks followed by the mass motions exhibiting the features of the spicule-like jets. The normalized velocity vectors are over-plotted on each density maps between $t=0$ s and $t=1000$ s. 86

3.4 Top Panel: The logarithm of mass density (ρ) in $g\ cm^{-3}$ with three dotted slits (case-1, case-2, case-3) is displayed. We estimate the distance-time diagrams over the chosen paths. Bottom Panel: The distance time diagrams corresponding to the chosen paths exhibit quasi-periodic rise and fall of the spicule-like cool jets. 87

3.5 Left column: The distance time diagram of the upward velocity (V_y) is shown along the chosen paths where jets are formed. Middle Column: The distance time diagram of V_z is displayed, which is scaled from -2.0 km s^{-1} to 2.0 km s^{-1} . These V_y and V_z are taken corresponding to the slits drawn on Fig. 3.4 (black-dotted lines) for three cases, i.e., case-1, case-2 and case-3. Right column: The temporal evolution of vertical velocity V_y (blue curve) and transverse velocity V_z (red curve) corresponding to the horizontal black slits on the left and middle columns respectively taken at $y=3.0$ Mm. 88

- 3.6 The distance time diagram of the mass flux during the evolution of spicule-like jets is shown in the solar atmosphere (top-row). These diagrams correspond to the slits on Fig. 3.4, upper panel (black-dotted lines) for the three cases (i.e., case-1, case-2 and case-3). The over-plotted black-dashed lines on each map (top-row) show the paths where we estimate the mass flux w.r.t. the length of the jet. The spatial distributions of the mass flux of various jets are shown in rows 2 to 5 during their maximum elongation in the upward direction. 89
- 3.7 The distance time diagrams of the kinetic energy density (KED) are shown in the top panels during the evolution of spicule-like jets in the solar atmosphere. These diagrams correspond to the slits as shown on Fig. 3.4 upper-panel (black-dotted lines) for three cases (i.e., case-1, case-2 and case-3). The over-plotted black-dashed line on each maps (top row) show the path where we estimate the KED w.r.t. the length of the first jet. The bottom row displays the spatial distributions of KED associated with the first spicule-like jets (P11, P21, P31) during their maximum elongation in the upward direction. 90
- 3.8 The temporal evolution of the upward velocity (V_y) in the solar atmosphere (blue curve) is plotted corresponding to the horizontal black slits as shown on the left-most panels of Fig. 3.5. These slits are drawn there at $y = 3.0$ Mm. The temporal evolution of the mass flux (red curve) corresponding to the black dotted horizontal line as chosen on Fig. 3.6 (top row) at $y = 3.0$ Mm is also compared for the three cases (i.e., case 1, 2 and 3). 91
- 3.9 The wavelet analysis of the temporal variation of the mass flux launched by various spicule-like jets along each chosen paths (i.e., case 1-3). The mass flux variation is estimated at the coronal height of 3.0 Mm. 92

-
- 4.1 Equilibrium open and expanding magnetic field lines in the model quiet-Sun solar atmosphere. 108
- 4.2 Temperature variation with the height in the initial static solar atmosphere. 109
- 4.3 Magnetic field profile (left) and plasma-beta profile (right) vs. height (y) in the model quiet solar atmosphere. 111
- 4.4 Equilibrium profiles of mass density (left) and gas pressure (right) vs. height in the model quiet solar atmosphere. 111
- 4.5 Sound speed (left) and Alfvén speed (right) vs. height (y) in the model quiet solar atmosphere. 112
- 4.6 Evolution of the plasma jets at different pressure pulse in two different strength of the magnetic fields $B=56$ Gauss and $B=112$ Gauss. The Mosaic diagram shows the maximum height of the evolved jets at different pressure pulses, e.g., $A_p = 4-22$. Horizontal (x) and vertical (y) axes are in Mm. . . 115
- 4.7 Automated detection of the plasma jet in the numerical simulation data to establish its time-distance profile and termination point. 117
- 4.8 Height of the jets and their evolution w.r.t. the time. 117
- 4.9 Maximum height of the model jets vs. pressure pulse strength. 118

- 4.10 Top-panel: The example spatial profiles of various jets when they reach at their respective maximum height In the top-panel, figures 'a', 'b', 'c' respectively show spatial profiles of the jet at $B=56$ Gauss, $A_p=16$; $B=56$ Gauss, $A_p=6$, $B=112$ Gauss, $A_p=18$. Since the base of these jets exhibits complex shape, therefore, the triple or single Gaussian profiles are fitted and the respective FWHMs are estimated after determining the Gaussian width. Bottom-panel: Width of the jets vs. pressure pulse strength (A_p) in the solar atmosphere for magnetic field $B=56$ Gauss (blue-diamonds) and $B=112$ Gauss (red circles). The FWHM of various jets lie between 0.42 to 0.48 Mm. They show mild increasing trend though for both the magnetic fields. 119
- 4.11 Life-time of the model jets vs. pressure pulse strength. 120
- 5.1 The observational data demonstrates (a): SJI 1330 Å image taken at 21:41:30 UT. The red-dashed line in (a) displays the associated spicule-like jet. (b): Temporal evolution of the peak intensity of Si iv 1393.755 Å line profiles. The vertical purple line shows the time of panel (a). The yellow diamonds indicate velocity enhancements in form of two comparable peaks or enhancement in both the wings, while the blue (red) diamonds indicate such enhancement at only the blue (red) wing. (c): Line profile at the intersection of the horizontal dashed line and vertical purple line shown in panel (b). The dashed black line represents the single Gaussian fit. (d): Wavelength (in velocity)–time diagram of the Si iv 1393.755 Å line. . . . 133
- 5.2 Left-panel: Equilibrium unipolar magnetic field vectors in the model solar atmosphere. Right-panel: Temperature profile derived from the model of (Avrett and Loeser, 2008). 137

- 5.3 The physical properties of the solar atmosphere and their variations with respect to (w.r.t.) height (y) in its equilibrium condition. The top row shows the variation of magnetic field (left), mass density (middle), and gas pressure (right) along the vertical direction of the solar atmosphere. The bottom row illustrates the variation of plasma-beta, Alfvén speed, and sound speed vs. y . The typical values of these characteristic parameters and speeds are well suited for the magnetized solar atmosphere. 137
- 5.4 Spatio-temporal evolution of the cool spicule-like jet as shown in the temperature maps: First to fourth rows respectively display evolution of the representative model jet in the solar atmospheres under adiabatic condition, thermal conduction, radiative loss, and combined effect of thermal conduction and radiative loss. The velocity vectors are scaled upto the maximum velocity of 100 km s^{-1} as overplotted on different maps. . . 141
- 5.5 Synthetic images in Si IV 1393.755 \AA using the simulation data at $t=180$ s, and CHIANTI Atomic Database: (a) the adiabatic condition (top-left panel); (b) thermal conduction (top-right panel); (c) the radiative loss (bottom-left); (d) joint effect of thermal conduction and radiative loss (bottom-right panel). 142
- 5.6 Distance time diagrams in density (left-column) and temperature (right-column) of the model jet. The first to fourth rows respectively represent an adiabatic condition, thermal conduction, radiative loss, and combined effect of thermal conduction and radiative loss. 144

- 5.7 The distance time maps of the kinetic energy density (KED) (1st column) and mass flux (MF) (3rd column) are shown during the evolution of jet in the corona. The first row of the panels are related to the estimations in the adiabatic case, second row when only thermal conduction is added, third row when only radiation losses are included, and fourth row when both thermal conduction and radiative losses are considered. The black-dashed paths are overplotted on each of these maps (the 1st and the 3rd column). The KED and MF are estimated w.r.t. the length of the jet along these chosen paths (the 2nd and the 4th column). The spatial distribution of the KED and MF along the jet is basically the manifestation of their values at different temporal epochs when jet is traveling upward. 145
- 5.8 Time signatures of mass flux (left-panel) and energy flux (right-panel) estimated at height $y=5.0$ Mm for adiabatic (black), thermal conduction (blue), radiative loss (red), and combined effect of thermal conduction plus radiation (magenta). 146
- 6.1 Left: The equilibrium magnetic field lines in the stratified model solar atmosphere. The null point formed above the TR in lower corona. Right: The variation of temperature (T) (blue-curve) and mass density (ρ)(red curve) w.r.t. vertical direction (y) in the model solar atmosphere. 170
- 6.2 The mass density (ρ) profile with six dotted slits chosen on the cool jets J₁ and J₂', where we estimate the distance–time diagrams over these chosen slits. The FoV demonstrates the evolution of various cool jets and plasma flows. 176

6.3 The normalized density map of the evolution of cool jets. The jet J_1 and J_2 as highlighted in Fig. 6.2. These cool jets are triggered by the implementation of random vertical velocity (V_y) pulses initially. The pulses are applied in the chromosphere between 1.0 and 1.5 Mm. The normalized velocity vectors are over-plotted on each density map between $t = 0$ and 820 s. 177

6.4 Left: The distance-time diagrams in density for the jet ' J_1 ' corresponding to the slits S11, S12 and S13 in Fig. 6.2. These diagrams show the decaying kink waves in the jet ' J_1 '. They also display the radial structuring of the density across the oscillating jet. Right: The distance-time diagrams in Alfvén velocity for jet ' J_1 ' corresponding to the slits S11, S12 and S13 as shown in Fig. 6.2. These maps clearly demonstrate the radial structuring of the Alfvén speed across the oscillating jet. 178

6.5 Left: The distance-time diagrams in density for jet ' J_2 ' corresponding to the slits S21, S22 and S23 as shown in Fig. 6.2. These diagrams show the decaying kink oscillations in jet ' J_2 ', which quickly seized in one cycle. These diagrams also display the radial structuring of the density across the oscillating jet. Right: The distance-time diagrams in Alfvén velocity for jet the ' J_2 ' corresponding to the slits S21, S22 and S23 as shown in Fig. 6.2. These maps clearly demonstrate the radial structuring of the Alfvén speed across the oscillating jet. 178

6.6 Top row represents the density vs length, middle row the magnetic field vs length, and bottom row the Alfvén speed vs length of the slits S11 (for Jet J_1) (right column) and S21 (for jet J_2) (left column) at $t=800$ s. This clearly demonstrates that when we move radially outward the density decreases while the magnetic field and Alfvén speed increase. 179

- 7.1 Multi-temperature view of the fan-spine topology in hot and cool plasma as displayed in the *SDO/AIA* 94 Å, 131 Å, 193 Å, 304 Å filters at 08:05 UT on 2015 March 10. A dome-shaped fan-spine topology is visible in hot wavebands (e.g., 94 Å, 131 Å), while the K-H unstable vortices and two different layers appeared in the cool wavebands (e.g., 304 Å) and at typical coronal temperature e.g., 171 Å, 193 Å). Multithermal K-H unstable vortices have indicated by the cyan-color arrows. 190
- 7.2 The sequence of images of *SDO/AIA* 304 Å shows the two layers of plasma flow and the onset of K-H instability. Two layers of plasma flows are indicated by the L1 and L2. Different cyan-colored arrows indicate the K-H unstable vortices. 191
- 7.3 The region of interest (ROI; black box in Fig. 7.2) is shown by *SDO/AIA* 304 Å filter. Two plasma flow layers are indicated by "L1" and "L2" as indicated by the blue and cyan color dotted lines. Initially, the boundary of these two flows is smooth; however, when the interaction of two layers starts, it becomes a sawtooth pattern. Cyan-colored arrows indicate that the K-H unstable vortex develops in the lower flow layer (L2). Later, the K-H unstable vortices merged within each other, and again boundary became smooth. 193

7.4 A schematic shows the dynamical evolution of multi-layer plasma flow inside the ambient hot spine and the overall magnetic configuration of the fan-spine topology. The green color lines indicate the outer spine associated magnetic field. The yellow color lines collectively define the fan surface. The magnetic field lines (yellow) approach the null point. The null point is lying above the fan surface and has indicated by the red line. A thin layer of cool plasma (layer L1) lifts and flows along the elongated length of the spine. This layer reaches the highest height, and after that, the second layer of plasma flow starts (L2; brown dotted line lying inside the green outer spines). At the highest height of the spine, the two-layer of plasma flow propagates in opposite directions. A layer of invisible material separates the two layers of plasma (blue and brown). At this invisible surface, multiple K-H unstable vortices appeared due to the velocity difference. 194

7.5 Left panel: We select the slit along the interface of the two plasma flow to estimate the velocity of the ejected plasma. Right panel: We track the path of ejected plasma in the H–T diagram to measure the velocity of the K-H unstable vortices, velocity of the upper layer, and shearing or velocity difference between two layers. 195

7.6 DEM map at different temperatures of $\log T=5.7-7.2$ at 08:05:32 UT when the K-H unstable vortices fully develop. Multi-thermal and multi-layer of plasma flow are evident in the fan-spine configuration. The K-H unstable vortices and flow inside the spine are primarily visible in coronal temperature ($\approx \log T=5.7-6.4$), and fan-spine topology is evident in the hot channel ($\log T=6.8-7.2$). We select two box regions to deduce the mass density in the two layers of plasma flow. 195

-
- 7.7 The region of interest (ROI; white box in Fig. 7.8) is displayed using *SDO/AIA* 304 Å images at 08:05:32 UT on 2015 March 10 when the K-H unstable vortices are completely evolved. The reverse color contrast is used to understand the evolution of sheared plasma vortices as well as the launch of the magnetic twists at different epochs. 196
- 7.8 Left panel: The composite image of *SDO/AIA* 94+304 Å shows the simultaneous presence of the hot and cool plasma in the fan-spine configuration. The hot loops are already present in the ambient corona. The K-H unstable cool plasma traps within the outer spine of the fan-spine topology. A vertical path has been selected along the width of the spine to estimate the approximate width of the magnetic and velocity sheared layer. Right panel: Hight-time diagram along the width of the spine. 197

List of tables

1.1	The physical properties of the Sun (Credit: Priest 2014)	3
1.2	A list of the main characteristics of the chromospheric jets (e.g., spicules, mottles, and fibrils) based on their recent observations. (Credit: Skirvin et al. 2022)	21
2.1	IRIS observations in different passband with corresponding ions and temperature (Credit: LMSAL, NASA/IRIS).	47
2.2	The details of Visible, UV and EUV channels of SDO/AIA instrument with the primary emitting ions and their formation temperature in the solar atmosphere (Credit: NASA/SDO)	50
2.3	Coordinate systems implemented in the PLUTO code regarding the position coordinates, volumes and areas and their meanings in the Cartesian coordinate system (Credit: Mignone et al. (2007a))	61
6.1	Fitting parameters of the kink oscillations in jets (J_1 and J_2)	181

Nomenclature of Symbols

R_{\odot}	Radius of the Sun
M_{\odot}	Mass of the Sun
ρ	Mass density
L_{\odot}	Radiation Luminosity of the Sun
g	Solar gravity
K_B	Stefan-Boltzmann constant
κ	Opacity
n	Number density
v_A	Alfvén velocity
v_s	sound speed
p	plasma pressure
β	plasma beta
η	Magnetic diffusivity
k	Wave vector
θ	Angle between the magnetic field (B) and wave vector
A	Atwood number
R_m	Reynolds number
R_i	Temperature response
γ_{Obs}	Observed growth rate
γ_{Th}	Theoretical growth rate
λ	Characteristic wavelength of the KH instability